Conformational changes induced by chaperone interactions facilitate lipid transport critical for bacterial outer membrane asymmetry

Jiang Yeow[1] and Shu-Sin Chng[1,2,*]

Affiliation:

[1]Department of Chemistry, National University of Singapore, Singapore 117543

[2]Singapore Center for Environmental Life Sciences Engineering, National University of Singapore (SCELSE-NUS), Singapore 117456

[*]To whom correspondence should be addressed: chmchngs@nus.edu.sg

Author Contributions: J.Y. and S.-S.C designed research; J.Y. performed wet lab experiments described in this work; J.Y. and S.-S.C. analyzed and discussed data; J.Y. and S.-S.C. wrote the paper.

Competing Interest Statement: The authors declare no competing interests.

Classification: Biological Sciences; Biochemistry

Keywords: bacteria; outer membrane; lipid transport; phospholipid; lipid asymmetry; membrane protein; protein complex; channel

This PDF file includes:

Main Text

Figures 1 to 6

Abstract

The outer membrane (OM) of Gram-negative bacteria is an asymmetric lipid bilayer with outer leaflet lipopolysaccharides (LPS) exposed to extracellular milieu and inner leaflet phospholipids (PLs) facing the periplasm. This unique lipid asymmetry is the key to its innate drug resistance, rendering the OM impermeable to external insults, including antibiotics and bile salts. To maintain this OM barrier, the OmpC-Mla system removes mislocalized PLs from the OM outer leaflet, and transports them back to the inner membrane (IM); in the first step, the OM OmpC-MlaA complex transfers PLs to the periplasmic chaperone MlaC. This process likely occurs via a hydrophilic channel in MlaA, yet mechanistic details have remained elusive. Here, we obtain a molecular view of the architecture of the MlaA-MlaC transient complex by mapping the interaction surfaces between MlaA and MlaC in *Escherichia coli*. We show that electrostatic interactions are important for MlaC recruitment, and that MlaC eventually binds MlaA at the periplasmic face in a manner that juxtaposes the MlaA channel and the MlaC lipid binding cavity. We further provide evidence for conformational changes in the MlaA channel that correlate with functional states of MlaA, as well as interactions with MlaC binding and OM porins. Our work offers novel insights into the molecular mechanism for lipid transfer by the OmpC-MlaA complex for overall retrograde transport of PLs to the IM to maintain OM lipid asymmetry.

41 **Introduction**

42 Gram-negative bacteria assemble two lipid bilayers in their cell envelopes - the inner membrane (IM)
43 and the outer membrane (OM) that encapsulate the cytoplasm and periplasm, respectively. At the OM,
44 lipopolysaccharides (LPS) pack tightly with divalent cations and occupy the outer leaflet, while phospholipids
45 (PL) reside mostly in the inner leaflet, presenting a unique bilayer with extreme asymmetry (1-3). The outer
46 leaflet of LPS forms a stable layer with drastically reduced permeability, offering an effective protective
47 barrier against the entry of toxic compounds, such as detergents and antibiotics. Proper establishment and
48 maintenance of lipid asymmetry is thus critical for OM barrier function, which allows Gram-negative bacteria
49 to survive in the most hostile environments, including the mammalian intestinal tract.

50 How OM lipid asymmetry is achieved has been extensively studied. It is well known that LPS are
51 transported and inserted into the outer leaflet of the OM via the Lpt protein bridge machinery (4). Other major
52 OM components, i.e. β-barrel proteins and OM lipoproteins, are assembled into the membrane via the Bam
53 (5) and Lol (6) pathways, respectively. It is less understood how exactly PLs are brought to the OM (7), but
54 recent studies suggest the involvement of a redundant set of AsmA-like proteins in this process (8-10).
55 Evidently, balancing the levels of all these OM components during active cell growth and division would be
56 critical to ensure OM stability, and hence lipid asymmetry. In this regard, the Tol-Pal complex has been
57 implicated in lipid homeostasis, possibly via removal of excess PLs from the OM (11). When coordination
58 across these pathways is sub-optimal, PLs may become mislocalized to the outer leaflet of the OM, forming
59 PL bilayer patches that compromise OM lipid asymmetry and barrier function (12, 13). To cope with these
60 defects, additional cellular mechanisms are deployed to eliminate PLs that end up aberrantly in the outer leaflet
61 of the OM. The OM phospholipase, PldA, hydrolyzes acyl chains from these PLs (14), while the OM
62 acyltransferase, PagP, transfers an acyl chain from outer leaflet PLs to LPS and phosphatidylglycerol (PG)
63 (15, 16). Finally, the OmpC-Mla system, an established PL trafficking pathway, extracts PLs from the outer
64 leaflet of the OM and shuttles them back to the IM (17, 18).

65 The OmpC-Mla system, first identified in *Escherichia coli* based on homology to the TGD2 pathway
66 in *Arabidopsis thaliana*, comprises the OM lipoprotein MlaA in complex with osmoporin OmpC, the
67 periplasmic chaperone MlaC, and the IM ATP-binding cassette (ABC) transporter MlaFEDB (17-19).

68 Removing *ompC* or any *mla* component results in PL accumulation in the outer leaflet of the OM of *E. coli*,
69 indicating a role in maintaining OM lipid asymmetry (17, 18). To achieve that, the OmpC-MlaA complex
70 somehow extracts PLs from the outer leaflet of the OM, hands them over to MlaC, which in turn transfers
71 these PLs into the IM via the MlaFEDB complex (20-22). Many recent biochemical and structural studies
72 have provided detailed insights into ATP-dependent PL transfer steps at the IM (19, 20, 23-30). In particular,
73 we now know that when PL-bound MlaC arrives at the IM, it can spontaneously transfer the lipid molecule to
74 the binding cavity of MlaFEDB (21). Even though this initial process is reversible (20, 21, 25), ATP
75 binding/hydrolysis by the MlaFEDB complex ultimately catalyzes the transfer of PLs into the IM, driving
76 overall retrograde transport from the OM (20, 21). How ATP binding/hydrolysis may be coupled to PL
77 transport in the MlaFEDB complex can be partly inferred from recently solved structures (20, 26-30), though
78 detailed mechanistic understanding is still limited.

79 Lipid transfer at the OM is somewhat less understood, especially how retrograde PL movement from
80 the outer leaflet of the OM to MlaC can be facilitated in an energy-independent manner. The OM lipoprotein
81 MlaA interacts with trimeric porins OmpC and OmpF, where OmpC appears to play a more critical role in
82 Mla function (18). It has been established that, unlike canonical lipoproteins, MlaA resides entirely within the
83 OM bilayer and makes extensive contacts with porins at their dimeric interfaces. Moreover, MlaA itself forms
84 a hydrophilic channel in the OM, which may be gated by conformational movements of an adjacent β-hairpin
85 loop motif (31, 32). The MlaA channel may provide a plausible path for PL translocation across the OM;
86 however, we do not yet have clear ideas of how MlaA actually sits in the OM lipid bilayer, as well as the
87 expected conformational changes that should occur in the protein during PL transport. MlaC binds PLs with
88 presumed high affinity (24, 25, 33), and has been demonstrated to interact with MlaA in vivo (24) and in vitro
89 (23). Yet it remains elusive how exactly MlaA interacts with MlaC to allow spontaneous, productive transfer
90 of PLs.

91 Here, we elucidate a molecular picture of the transient MlaA-MlaC complex during PL transfer at the
92 OM. Using in vivo photo- and disulfide-crosslinking, we demonstrate that MlaC interacts with MlaA directly
93 at its periplasmic base, in a manner that juxtaposes the lipid binding cavity of MlaC with the hydrophilic
94 channel of MlaA. In addition, mutational analyses reveal that MlaA recruits MlaC to the OM via additional

electrostatic interactions between a C-terminal tail helix of MlaA and a surface charged patch on MlaC, an observation corroborated by an AlphaFold2 predicted model of the interaction complex. Furthermore, we establish solvent-accessibility changes in a key channel residue in MlaA that are influenced by interactions with MlaC and porins (OmpC/F), as well as functionality of MlaA itself. Collectively, our work provides mechanistic insights into how MlaC interacts with MlaA to induce conformational changes that may facilitate retrograde PL transfer from the outer leaflet of the OM to MlaC to maintain lipid asymmetry.

Results

MlaC interacts with α-helices at the periplasmic opening of the hydrophilic channel of MlaA

To receive PLs from MlaA, MlaC would have to gain access to the hydrophilic MlaA channel from the periplasmic side, albeit transiently. To map the region(s) on MlaA that contacts MlaC, we replaced ~27 residues on the periplasmic face of *E. coli* MlaA separately with *para*-L-benzoylphenylalanine (*p*Bpa) (34), and examined which positions allow photoactivatable crosslinks with MlaC. We found five positions on MlaA that demonstrated strong photoactivatable crosslinks with MlaC when substituted with *p*Bpa (**Fig. 1A and 1B**). Another five positions exhibited weaker crosslinks to MlaC (**Fig. S1**). Interestingly, these residues are all located on the C-terminal helices (Q195-N226) of MlaA extending from the channel opening in the periplasmic face (**Fig. 1C**), suggesting that MlaC can be juxtaposed to receive lipids from MlaA at the base of the channel.

We have also previously established the residues on MlaC that contact MlaA via the same photocrosslinking approach (24). To determine reciprocal contact points between the two proteins, we introduced cysteines at positions on either protein that displayed strong photoactivatable crosslinks, and monitored disulfide bond formation between these MlaA and MlaC cysteine variants in cells. We tested 24 combinations of cysteine residue-pairs from four and six positions on MlaA and MlaC, respectively. Of these pairs, 11 enabled disulfide bond formation between MlaA and MlaC, indicating that these residue positions can lie in close proximity when the two proteins interact (**Fig. 2A**). $MlaA^{Q195C}$ and $MlaC^{Q151C}$ did not form disulfide crosslinks with any partner cysteine variants tested. In contrast, Q205, M212 and F223 on MlaA, and K128, S172 and T175 on MlaC, each allowed disulfide bond formation with multiple tested positions on

122 their partner protein, when replaced with cysteine (**Figs. 2A and 2B**). The strongest disulfide crosslink was
123 MlaA^{Q205C}-MlaC^{V171C} (**Figs. 2A and S2**), highlighting perhaps a major interaction mode in the transient
124 complex. Interestingly, Q205 lies directly at the base of the hydrophilic channel of MlaA while V171 is
125 positioned at the entrance of the lipid binding cavity of MlaC (**Fig. 2B**), reflecting an approximate arrangement
126 that could lead to productive lipid transfer.
127

128 **Electrostatic interactions between the C-terminal tail helix of MlaA and a surface charged patch on**
129 **MlaC are necessary for MlaC recruitment**

130 We have shown that MlaC interacts with the C-terminal α-helices at the base of MlaA. However, there
131 is presumably an unstructured region beyond these interacting helices (G227-E251; *E. coli* numbering)
132 missing from the reported MlaA crystal structures (32); yet, in the recent structural model predicted by
133 AlphaFold (AF-P76506-F1) (35), the extreme end (N238-E251) of this 'tail' region was confidently modelled
134 as a short α-helix (**Fig. 3A**). To understand if this C-terminal tail helix is also important for MlaC interaction,
135 we made several MlaA deletion constructs, and probed for MlaC interaction. While removing residues after
136 P232 (MlaA^{CTD4}) conferred milder SDS/EDTA sensitivity than cells lacking MlaA (**Fig. S3A**), it had
137 completely abolished disulfide bond formation between MlaA^{Q205C} and MlaC^{V171C} (**Fig. 3B**). In fact, deletion
138 of the last 9 amino acids on MlaA^{D243X} (MlaA^{CTD6}), a highly negatively charged segment on the putative
139 terminal helix, was sufficient to disrupt disulfide crosslinks with MlaC. To test the importance of
140 electrostatics, we also constructed two sets of Arg mutants at a single face of this helix, MlaA$^{D243R/D244R}$
141 (MlaA^{2DD2R}) and MlaA$^{D247R/E251R}$ (MlaA^{2DE2R}) (**Fig. 3A**), and found that these charged-reversed variants
142 drastically reduced disulfide crosslinks between MlaA^{Q205C} and MlaC^{V171C} (**Fig. 3B**). The different MlaA
143 variants are still able to pull down trimeric OmpC, indicating they preserve overall MlaA structure (**Fig. S4**).
144 We conclude that the negatively-charged residues on the C-terminal tail helix of MlaA are also critical for
145 MlaC interaction.

146 We next asked if there are specific positively-charged regions on MlaC that interact with the C-
147 terminal tail helix of MlaA. We identified seven clusters of positively-charged residues (Arg/Lys) all around
148 the structure of apo-MlaC (25) (**Fig. 4A**), and successfully converted five of these clusters to aspartates

149 separately. MlaC$^{K84D/R90D}$ (MlaC1) abolished disulfide crosslinks between MlaA^{Q205C} and MlaC^{V171C}, while
150 MlaC^{K71D} (MlaC0) and MlaC$^{R143D/R147D}$ (MlaC3) led to partial loss (**Fig. 4B**), confirming the overall
151 importance of electrostatics. These mutations did not introduce any SDS/EDTA sensitivity (**Fig. S3B**),
152 however, suggesting they may only impact recruitment efficiency, but not overall lipid transport function.
153 Remarkably, combining MlaA$^{D243R/D244R}$ (MlaA^{2DD2R}) with MlaC$^{K84D/R90D}$ (MlaC1) fully restored disulfide
154 bond formation (**Fig. 4C**), implying that residues D243/D244 on MlaA directly contact residues K84/R90 on
155 MlaC during MlaA-MlaC interaction.

156 To obtain a possible picture of the MlaA-MlaC interface, we applied AlphaFold2 to predict the
157 structural model of the MlaA-MlaC complex (35-37). Amazingly, the model not only revealed an arrangement
158 of MlaA and MlaC that is fully consistent with our in vivo crosslinking data (especially *p*Bpa), it also correctly
159 predicted the charge-charge interactions between the D243/D244 on MlaA and K84/R90 on MlaC (**Fig. 4D**).
160 The C-terminal tail helix of MlaA is connected to the rest of the protein via a flexible linker, suggesting that
161 this tail helix might serve as a bait to recruit apo-MlaC to the OM complex via electrostatic attraction.
162 Importantly, once MlaC is stably bound and positioned, the hydrophilic channel in MlaA becomes continuous
163 with the lipid binding cavity of MlaC (**Fig. 4D**), providing a glimpse into the route for PL transfer from the
164 outer leaflet of the OM to MlaC.

165

166 **Interactions with MlaC modulate conformational changes in the MlaA channel**

167 Productive MlaA-MlaC interactions would be required for PL transfer from the OmpC-MlaA complex
168 to MlaC. We hypothesize that such interactions could elicit conformational changes in MlaA to facilitate PL
169 transfer. To test this idea, we examined the solvent accessibilities, as an indication of possible conformational
170 states, of specific residues within the MlaA channel in the absence of MlaC (**Fig. 5A**). We have previously
171 shown using the substituted cysteine accessibility method (SCAM) that many hydrophilic residues in the
172 MlaA channel are fully accessible to a membrane-impermeable thiol-reactive reagent ((2-sulfonatoethyl)
173 methanethiosulfonate; MTSES) in wild-type cells. One exception is K184, which exhibited partial MTSES
174 accessibility when substituted with cysteine; within the MlaA population in wild-type cells, K184C is
175 accessible to MTSES in some MlaA molecules but not others, in comparable proportions (**Fig. 5B**).

176 Interestingly, removing MlaC resulted in K184C becoming MTSES-inaccessible in the entire population of
177 MlaA (**Fig. 5B**), an effect not seen for other channel residues tested (**Fig. S5**). This shift in accessibility of
178 K184C was reversed by expressing wild-type MlaC in trans, but not the charge-reversed MlaC1 variant that
179 disrupted MlaA-MlaC interactions (**Fig. 5C**). This suggests that interaction with MlaC is required for MlaA
180 to adopt the state where K184C is solvent accessible. Furthermore, we observed that K184C in MlaA also
181 became MTSES-inaccessible in the Δ*mlaD* strain (**Fig. 5B**). While MlaC is still present in this strain, it is
182 likely bound to PLs (i.e. holo form), given that off-loading of MlaC is not possible in the absence of an intact
183 ABC transporter in the IM. Overall, our results indicate that the binding and release of apo-MlaC may
184 influence the solvent accessibilities and conformational states of the MlaA channel.

185 We have also considered the possibility that shifts in MTSES-accessibility could be due to OM
186 asymmetry defects in these *mla* strains. This is unlikely, however, since K184C MTSES-accessibility in other
187 OM-defective strains (Δ*tolB,* Δ*pal*) (11) was similar to that in wild-type cells (**Fig. S5A**). Supporting this
188 observation, the overexpression of phospholipase PldA, which can rescue OM asymmetry defects in *mla*
189 mutants (17), was unable to reverse the observed shifts in accessibility of K184C in both Δ*mlaC* and Δ*mlaD*
190 strains (**Fig. S5B**). We conclude that accessibility changes in K184 in MlaA are not due to the general loss of
191 lipid asymmetry in the OM.

192

193 **Non-functional MlaA variants adopt conformational states that no longer respond to interactions with**
194 **MlaC**

195 It is intriguing that K184C exhibits accessibility changes that may reflect different conformational
196 states in the MlaA channel, possibly due to functional interactions with apo-MlaC. We next asked whether
197 this same residue can also help us discern the functionality of MlaA itself. We first examined the MTSES-
198 accessibility of K184C in known MlaA variants. $MlaA^{G141P/G143P/G145P}$ ($MlaA^{3G3P}$) is a non-functional variant
199 believed to have restricted flexibility in a β-hairpin loop that may gate the MlaA hydrophilic channel (31).
200 $MlaA^{\Delta N43F44}$ (MlaA*) is a gain-of-function variant that is thought to have poor control of loop dynamics,
201 resulting in PL flipping from the inner to the outer leaflet of the OM (8, 31, 38). Interestingly, K184C in the
202 entire population of $MlaA^{3G3P}$ or MlaA* appeared to be fully accessible to MTSES in cells, contrary to that

203 observed in wild-type MlaA (**Fig. 5D**). Furthermore, removing MlaC or MlaD did not alter the accessibility
204 of K184C in both MlaA variants, suggesting that $MlaA^{3G3P}$ and MlaA* are in conformational states that cannot
205 respond to interactions with apo-MlaC. Both $MlaA^{3G3P}$ and MlaA* are therefore non-functional in facilitating
206 retrograde PL transfer to MlaC.

207 An outstanding question in the OmpC-Mla system relates to why only OmpC, but not OmpF, appears
208 to function together with MlaA. Under high osmolarity conditions, OmpC is produced at higher levels than
209 OmpF (18). Therefore, to gain insights into the role of porins in the pathway without confounding effects due
210 to expression levels, we went on to examine the solvent accessibility of MlaA K184C in the Δ*ompC* Δ*ompF*
211 double mutant complemented in trans with either *ompC* or *ompF*. Interestingly, removing both OmpC and
212 OmpF completely shifted the $MlaA_{K184C}$ population to a MTSES-accessible state (**Fig. 5E**), and expressing
213 OmpC or OmpF in trans (at comparable levels, **Fig. S6**) restored the population of $MlaA_{K184C}$ to liken that in
214 wild-type cells. These results indicate that free MlaA may not adopt a native conformational state in the OM,
215 and that interactions with either porin is required yet sufficient for scaffolding MlaA. We further noted that
216 the $MlaA_{K184C}$ population in just the Δ*ompC* mutant was already fully MTSES-accessible, and this observation
217 was independent of the presence of MlaC (**Fig. 5F**). Overall, MlaA in strains lacking OmpC alone may also
218 mostly not be bound to porins (owing to low levels of OmpF), and therefore largely adopts a non-functional
219 conformational state, mirroring what we have observed in the MlaA variants. We conclude that interactions
220 with trimeric porins allow MlaA to adopt functional states important for lipid transport.

221

222 **Discussion**

223 How the OmpC-MlaA complex transfers PLs from the outer leaflet of the OM to MlaC, as part of the
224 role of the OmpC-Mla system in maintaining lipid asymmetry, is not known. In this study, we have mapped
225 the interacting surfaces between MlaA and MlaC, resolved the molecular architecture of the transient MlaA-
226 MlaC complex, as well as revealed conformational changes of MlaA during PL transfer to MlaC. Using
227 molecular cross-linking, we have shown that MlaC binds MlaA at its periplasmic face in a manner where the
228 lipid binding cavity of MlaC is aligned with the hydrophilic channel of MlaA to create a continuous path for
229 PLs. We have also demonstrated that electrostatic interactions between the C-terminal tail helix of MlaA and

230 a charged patch on MlaC are required for (initial) recruitment. Finally, we have uncovered that wild-type
231 MlaA adopts distinct conformational states that is likely modulated by interactions with (apo)-MlaC. Our work
232 provides a mechanistic glimpse of how PLs may be transferred across the MlaA channel into the MlaC binding
233 pocket for onward shuttling to the IM.

234 The requirement of electrostatic interactions between MlaA and MlaC allows us to infer a mechanism
235 for how MlaA ensures effective recruitment and binding of apo- over holo-MlaC, thereby facilitating overall
236 retrograde transfer of PLs. We have established that the positively-charged patch formed by residues K84/R90
237 on MlaC, and the negatively-charged C-terminal tail helix residues D243/D244 on MlaA, directly interact
238 (**Fig. 4**), and are important for MlaC recruitment. We note that residues K84/R90 on MlaC are exposed and
239 accessible on apo-MlaC (25). Remarkably, this positively-charged patch is somewhat occluded by movement
240 of a surface loop on MlaC upon PL binding (23) (**Fig. 6**), limiting access by the MlaA tail helix. Such
241 differential accessibility on MlaC likely allows preferential recruitment of apo-MlaC over holo-MlaC at the
242 OM (**Fig. 6**). Post-recruitment, additional interactions between MlaA and MlaC occur at the base of the MlaA
243 hydrophilic channel, stabilizing the complex for productive PL transfer. Once MlaC picks up a PL molecule,
244 however, the charge-charge interaction with the MlaA tail helix is lost due to sterics (**Fig. 6**), leading to
245 possible destabilization of the MlaA-MlaC complex, and release of holo-MlaC from the OM. In a way, the
246 MlaA tail helix, possibly extended almost halfway into the periplasmic space via a flexible linker (25 residues,
247 ~88 Å), serves both as an electrostatic bait for MlaC during recruitment, and also a latch that locks down the
248 transient MlaA-MlaC complex during PL transfer. This could be a fascinating strategy to favor apo-MlaC
249 recruitment/binding, and may ensure that PL transfer takes place in a retrograde fashion.

250 In the context of MlaC binding and release, we can now also introduce a model for MlaA cycling
251 between distinct conformation states during PL transfer (**Fig. 6**). We have shown that MlaA exists in at least
252 two states in wildtype strains, where K184 is somehow accessible to the aqueous environment (State B), or
253 not (State A). Interestingly, K184 is positioned midway up the MlaA channel in the membrane, and close to
254 the gating loop; we therefore speculate that the MlaA channel may be open in State B, yet closed in State A.
255 In the absence of MlaC, or with disrupted MlaA-MlaC recruitment, all of MlaA appears to become confined
256 to State A (channel closed). Accordingly, apo-MlaC recruitment and binding is likely required to induce MlaA

257 to shift to the channel-open State B, allowing productive PL transfer. It is conceivable that holo-MlaC then no
258 longer binds MlaA in quite the same way as apo-MlaC, possibly explaining why MlaA also adopts a channel-
259 closed State A in the absence of MlaD, where all of MlaC is presumably in the holo-form. Such coordination
260 between apo-MlaC binding and conformational changes in wild-type MlaA may favor retrograde PL transfer
261 at the OM.

262 Conformational analysis using K184 accessibility also facilitated our understanding of non-functional
263 variants/states of MlaA. We have found that free MlaA (not in complex with porins), $MlaA^{3G3P}$ and MlaA*
264 variants all adopt conformation state(s) where K184 is fully solvent accessible and is no longer responsive to
265 the presence of MlaC (binding) (**Fig. 5**). Since K184 accessibility only produces binary output, however, free
266 MlaA and these variants may well have distinct conformations that still allow K184 to be accessible to the
267 aqueous environment. $MlaA^{3G3P}$ is believed to be a loop-locked non-functional mutant, while MlaA* is
268 thought to have lost control of its gating loop (31). Our study suggests that even though MlaA* has gain-of-
269 function possibly in allowing PLs to flip across the OM to the cell surface (8, 38), this variant is in fact non-
270 functional in the native role of MlaA. Consistent with this idea, it has recently been demonstrated that MlaA*
271 is unable to support retrograde PL transfer in vitro (20). We have also now demonstrated that MlaA requires
272 trimeric porins like OmpC and OmpF for scaffolding and possibly achieving functional conformations, thus
273 overall accounting for porin function in the Mla system (18). Curiously, we did not observe changes in K184
274 accessibility in a strain expressing $OmpC^{R92A}$ (**Fig. 5E**), a mutation at the dimeric interface of OmpC trimers
275 (where MlaA binds) that impacts OM lipid asymmetry (31). Therefore, beyond proper scaffolding of MlaA,
276 OmpC may play yet-to-be-identified roles that facilitate PL transport by MlaA.

277 Ultimately, the exact mechanism by which the OmpC-MlaA complex extracts mislocalized PLs from
278 the outer leaflet of the OM and transfers them to MlaC will require additional resolution into the various
279 conformational states we have revealed herein. Structural information of wild-type and mutant OmpC-MlaA
280 complexes in the context of a native lipid bilayer, with and without MlaC bound, would provide mechanistic
281 insights into the process. Given that OM lipid asymmetry is critical for overall barrier function, novel insights
282 into the OmpC-MlaA-(MlaC) complex will also guide us in developing useful strategies to inhibit the OmpC-
283 Mla pathway in the future.

Acknowledgements

J.Y. was supported by the National University of Singapore Graduate School of Integrative Sciences and Engineering Scholarship (ISEP). This work was supported by the Singapore Ministry of Health National Medical Research Council under its Open Fund Individual Research Grant (MOH-000145) (to S.S.C.). The authors declare no conflict of interest.

290 **References**

291 1. Kamio Y & Nikaido H (1976) Outer membrane of Salmonella typhimurium: accessibility of
292 phospholipid head groups to phospholipase c and cyanogen bromide activated dextran in the external
293 medium. *Biochemistry* 15(12):2561-2570.

294 2. Funahara Y & Nikaido H (1980) Asymmetric localization of lipopolysaccharides on the outer
295 membrane of Salmonella typhimurium. *J Bacteriol* 141(3):1463-1465.

296 3. Nikaido H (2003) Molecular basis of bacterial outer membrane permeability revisited. *Microbiol Mol*
297 *Biol Rev* 67(4):593-656.

298 4. Okuda S, Sherman DJ, Silhavy TJ, Ruiz N, & Kahne D (2016) Lipopolysaccharide transport and
299 assembly at the outer membrane: the PEZ model. *Nat Rev Microbiol* 14(6):337-345.

300 5. Konovalova A, Kahne DE, & Silhavy TJ (2017) Outer Membrane Biogenesis. *Annu Rev Microbiol*
301 71:539-556.

302 6. Okuda S & Tokuda H (2011) Lipoprotein sorting in bacteria. *Annu Rev Microbiol* 65:239-259.

303 7. Yeow J & Chng SS (2022) Of zones, bridges and chaperones - phospholipid transport in bacterial outer
304 membrane assembly and homeostasis. *Microbiology (Reading)* 168(4).

305 8. Grimm J*, et al.* (2020) The inner membrane protein YhdP modulates the rate of anterograde
306 phospholipid flow in Escherichia coli. *Proc Natl Acad Sci U S A* 117(43):26907-26914.

307 9. Ruiz N, Davis RM, & Kumar S (2021) YhdP, TamB, and YdbH Are Redundant but Essential for
308 Growth and Lipid Homeostasis of the Gram-Negative Outer Membrane. *mBio* 12(6):e0271421.

309 10. Douglass MV, McLean AB, & Trent MS (2022) Absence of YhdP, TamB, and YdbH leads to defects
310 in glycerophospholipid transport and cell morphology in Gram-negative bacteria. *PLoS Genet*
311 18(2):e1010096.

312 11. Shrivastava R, Jiang X, & Chng SS (2017) Outer membrane lipid homeostasis via retrograde
313 phospholipid transport in Escherichia coli. *Mol Microbiol* 106(3):395-408.

314 12. Jia W*, et al.* (2004) Lipid trafficking controls endotoxin acylation in outer membranes of Escherichia
315 coli. *J Biol Chem* 279(43):44966-44975.

316 13. Wu T, *et al.* (2005) Identification of a multicomponent complex required for outer membrane
317 biogenesis in Escherichia coli. *Cell* 121(2):235-245.
318 14. Dekker N (2000) Outer-membrane phospholipase A: known structure, unknown biological function.
319 *Mol Microbiol* 35(4):711-717.
320 15. Bishop RE (2005) The lipid A palmitoyltransferase PagP: molecular mechanisms and role in bacterial
321 pathogenesis. *Mol Microbiol* 57(4):900-912.
322 16. Dalebroux ZD, Matamouros S, Whittington D, Bishop RE, & Miller SI (2014) PhoPQ regulates acidic
323 glycerophospholipid content of the Salmonella Typhimurium outer membrane. *Proc Natl Acad Sci U*
324 *S A* 111(5):1963-1968.
325 17. Malinverni JC & Silhavy TJ (2009) An ABC transport system that maintains lipid asymmetry in the
326 gram-negative outer membrane. *Proc Natl Acad Sci U S A* 106(19):8009-8014.
327 18. Chong ZS, Woo WF, & Chng SS (2015) Osmoporin OmpC forms a complex with MlaA to maintain
328 outer membrane lipid asymmetry in Escherichia coli. *Mol Microbiol* 98(6):1133-1146.
329 19. Thong S, *et al.* (2016) Defining key roles for auxiliary proteins in an ABC transporter that maintains
330 bacterial outer membrane lipid asymmetry. *Elife* 5.
331 20. Tang X, *et al.* (2021) Structural insights into outer membrane asymmetry maintenance in Gram-
332 negative bacteria by MlaFEDB. *Nat Struct Mol Biol* 28(1):81-91.
333 21. Low WY, Thong S, & Chng SS (2021) ATP disrupts lipid-binding equilibrium to drive retrograde
334 transport critical for bacterial outer membrane asymmetry. *Proc Natl Acad Sci U S A* 118(50).
335 22. Low WY & Chng SS (2021) Current mechanistic understanding of intermembrane lipid trafficking
336 important for maintenance of bacterial outer membrane lipid asymmetry. *Curr Opin Chem Biol*
337 65:163-171.
338 23. Ekiert DC, *et al.* (2017) Architectures of Lipid Transport Systems for the Bacterial Outer Membrane.
339 *Cell* 169(2):273-285 e217.
340 24. Ercan B, Low WY, Liu X, & Chng SS (2019) Characterization of Interactions and Phospholipid
341 Transfer between Substrate Binding Proteins of the OmpC-Mla System. *Biochemistry* 58(2):114-119.

342 25. Hughes GW, *et al.* (2019) Evidence for phospholipid export from the bacterial inner membrane by the
343 Mla ABC transport system. *Nat Microbiol* 4(10):1692-1705.
344 26. Chi X, *et al.* (2020) Structural mechanism of phospholipids translocation by MlaFEDB complex. *Cell*
345 *Res* 30(12):1127-1135.
346 27. Coudray N, *et al.* (2020) Structure of bacterial phospholipid transporter MlaFEDB with substrate
347 bound. *Elife* 9.
348 28. Zhang Y, Fan Q, Chi X, Zhou Q, & Li Y (2020) Cryo-EM structures of Acinetobacter baumannii
349 glycerophospholipid transporter. *Cell Discov* 6(1):86.
350 29. Mann D, *et al.* (2021) Structure and lipid dynamics in the maintenance of lipid asymmetry inner
351 membrane complex of A. baumannii. *Commun Biol* 4(1):817.
352 30. Zhou C, *et al.* (2021) Structural Insight into Phospholipid Transport by the MlaFEBD Complex from
353 P. aeruginosa. *J Mol Biol* 433(13):166986.
354 31. Yeow J, *et al.* (2018) The architecture of the OmpC-MlaA complex sheds light on the maintenance of
355 outer membrane lipid asymmetry in Escherichia coli. *J Biol Chem*.
356 32. Abellon-Ruiz J, *et al.* (2017) Structural basis for maintenance of bacterial outer membrane lipid
357 asymmetry. *Nat Microbiol* 2(12):1616-1623.
358 33. Huang YM, *et al.* (2016) Molecular dynamic study of MlaC protein in Gram-negative bacteria:
359 conformational flexibility, solvent effect and protein-phospholipid binding. *Protein Sci* 25(8):1430-
360 1437.
361 34. Chin JW, Martin AB, King DS, Wang L, & Schultz PG (2002) Addition of a photocrosslinking amino
362 acid to the genetic code of Escherichiacoli. *Proc Natl Acad Sci U S A* 99(17):11020-11024.
363 35. Jumper J, *et al.* (2021) Highly accurate protein structure prediction with AlphaFold. *Nature*
364 596(7873):583-589.
365 36. Evans R, *et al.* (2021) Protein complex prediction with AlphaFold-Multimer.
366 *bioRxiv*:2021.2010.2004.463034.
367 37. Mirdita M, *et al.* (2022) ColabFold: making protein folding accessible to all. *Nat Methods*.

368 38. Sutterlin HA, *et al.* (2016) Disruption of lipid homeostasis in the Gram-negative cell envelope activates
369 a novel cell death pathway. *Proc Natl Acad Sci U S A* 113(11):E1565-1574.
370
371

372 **Figure legends**

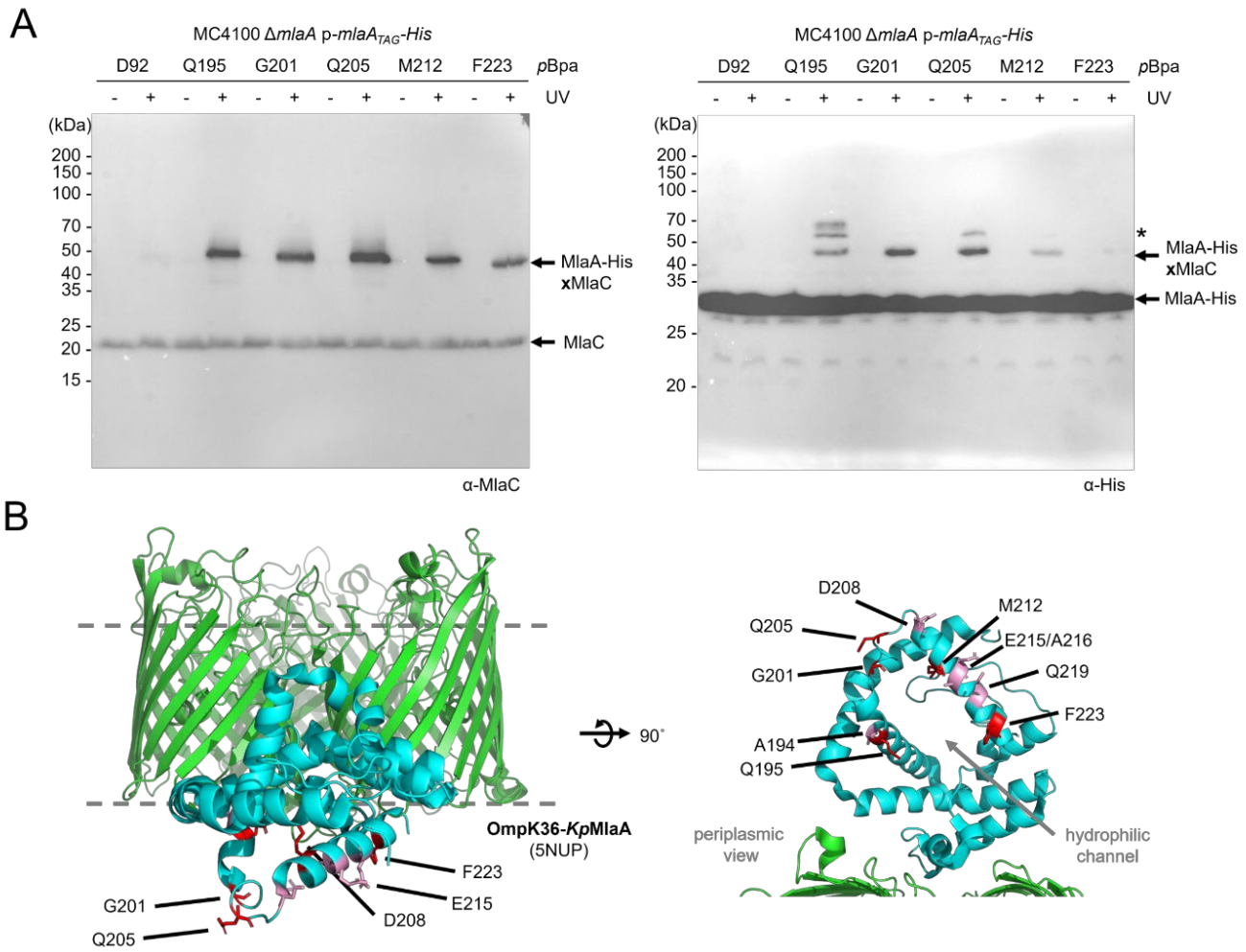

373

374 **Figure 1.** MlaA contacts MlaC in cells via C-terminal α-helices at the periplasmic opening of its hydrophilic
375 channel. (A) Representative immunoblots showing UV-dependent formation of strong crosslinks between
376 MlaA and MlaC in Δ*mlaA* cells expressing MlaA-His substituted with *p*Bpa at indicated positions from the
377 pCDF plasmid. Additional but unidentified MlaA$_{pBpa}$-His crosslinked adducts were detected and denoted with
378 an asterisk (*). (B) Membrane (*left*) and periplasmic (*right*) views of cartoon representations of the crystal
379 structure of *Klebsiella pneumoniae* OmpK36 (*green*)-MlaA (*cyan*) (PDB 5NUP) (32) with positions that
380 crosslink to MlaC highlighted. Residues exhibiting strong and weak photo-crosslinks with MlaC are illustrated
381 in *red* and *pink* sticks, respectively. The OM boundaries are indicated as *gray* dashed lines.

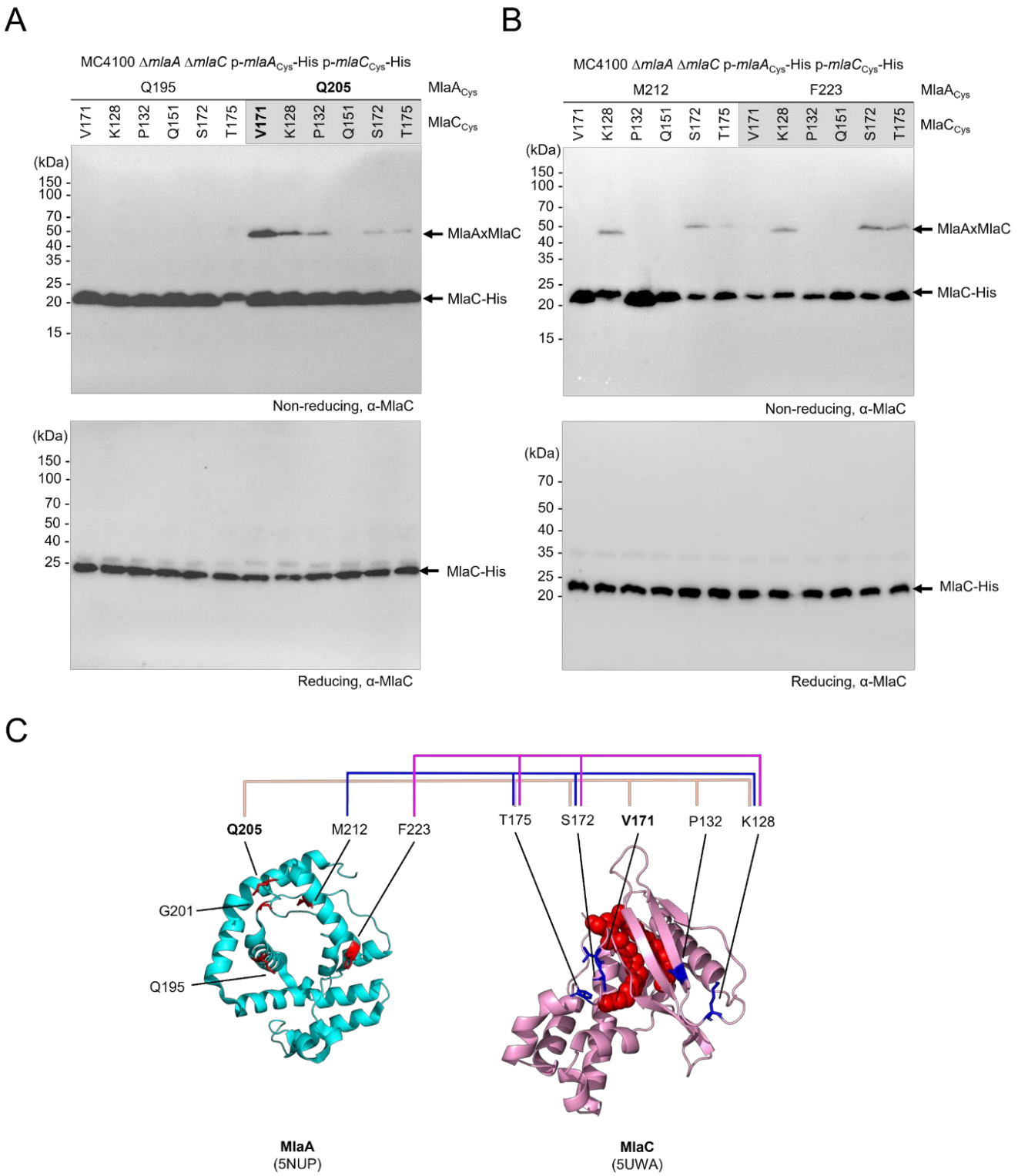

Figure 2. MlaC interacts with MlaA in a manner that juxtaposes the MlaA channel and the MlaC lipid binding cavity. (A) Representative immunoblots showing formation of disulfide crosslinks between MlaA and MlaC in Δ*mlaA* Δ*mlaC* cells expressing cysteine-substituted MlaA-His and MlaC-His from the pCDF and pET22/42 plasmids, respectively. Samples were subjected to non-reducing (*top*) or reducing (*bottom*) SDS-PAGE prior to immunoblotting. (C) Cartoon representation of *Kp*MlaA (*cyan*) (PDB 5NUP) (32) and holo-MlaC (*pink*, PL in

388 *red* spheres) (PDB 5UWA) (23). Residues on MlaC which displayed disulfide crosslinking with MlaA, and
389 vice versa, are illustrated in *red* and *blue* sticks, respectively. MlaC residues mapped to MlaA residues Q205C,
390 M212C and F223C are connected by *beige, blue* and *pink lines* respectively.
391

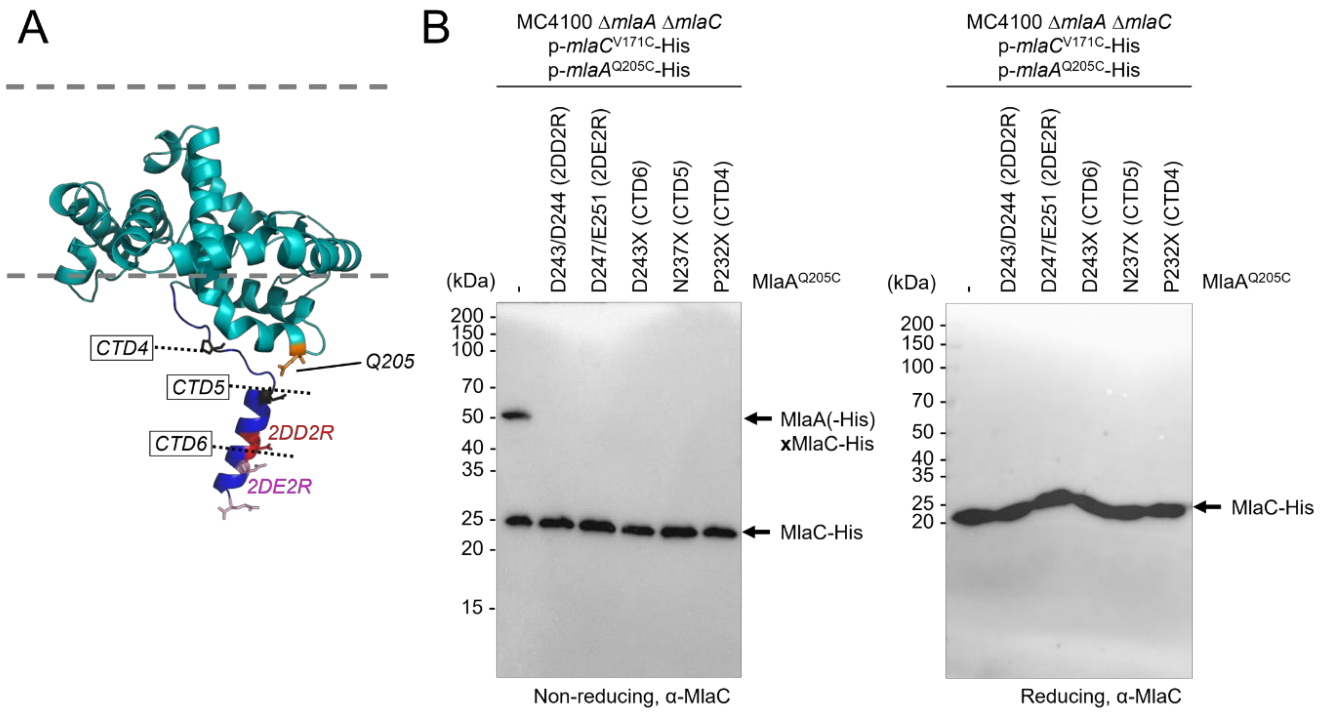

392

393 **Figure 3.** Negatively-charged residues on the putative C-terminal tail helix of MlaA are important for MlaC
394 recruitment. (A) Cartoon representation of the *Ec*MlaA (*teal*) model generated from AlphaFold (AF-P76506-
395 F1) (35) with the putative C-terminal tail helix coloured *blue*. C-terminal truncation positions (CTDs) are
396 annotated. MlaC-crosslinking residue Q205 is labelled in *orange* sticks. Charge-reversed residues in
397 MlaA^{2DD2R} and MlaA^{2DE2R} are labelled in *red* and *pink* sticks respectively. (B) Representative immunoblots
398 showing abolishment of disulfide crosslinks between MlaA and MlaC in Δ*mlaA* Δ*mlaC* cells expressing
399 various C-terminal tail helix mutants of MlaA^{Q205C}(-His) and MlaC^{V171C}-His from the pCDF and pET22/42
400 plasmids, respectively. Samples were subjected to non-reducing (*left*) or reducing (*right*) SDS-PAGE prior to
401 immunoblotting.

402

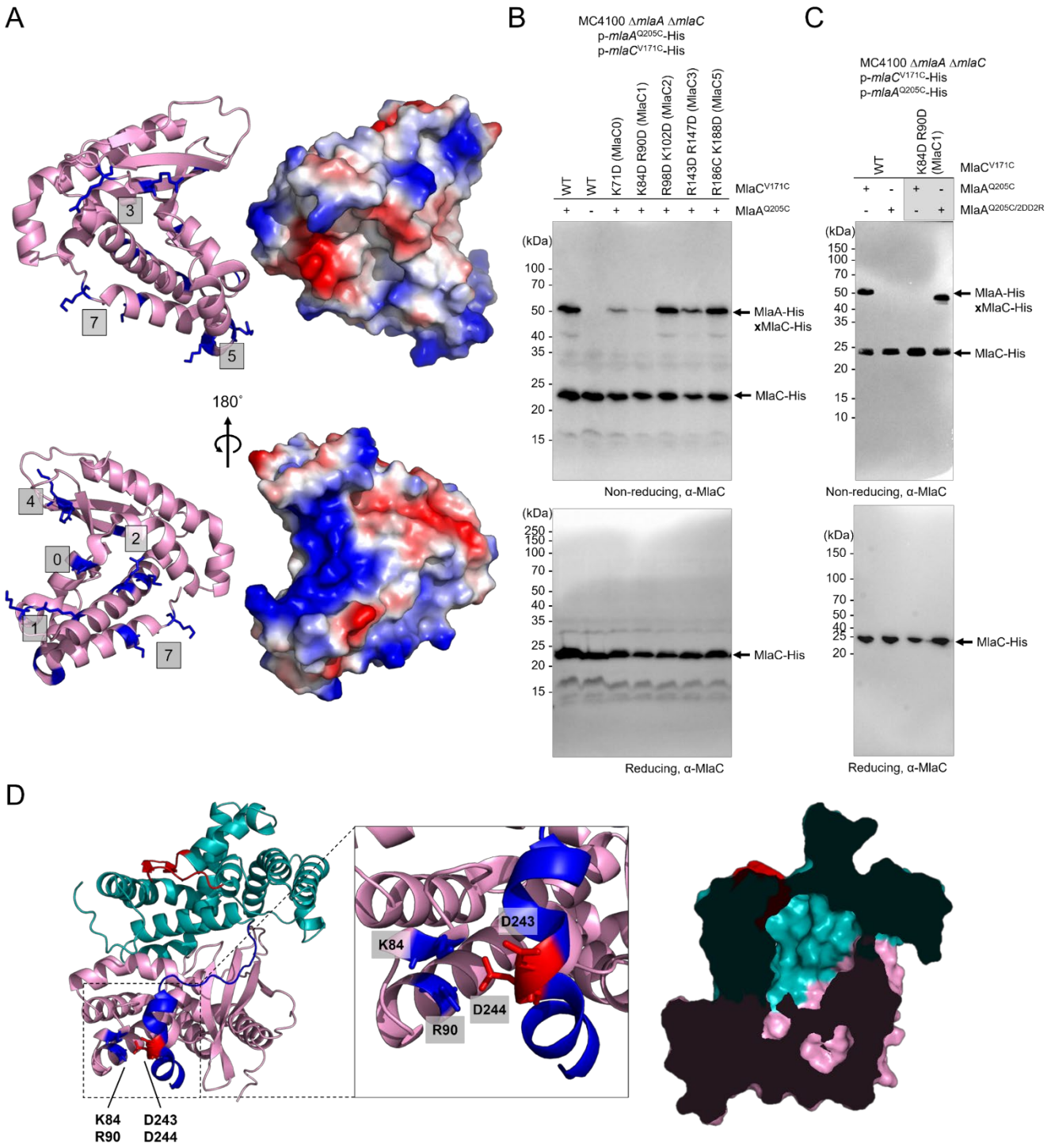

Figure 4. Positively-charged surface residues on MlaC are responsible for mediating MlaA interaction. (A) Cartoon and surface vacuum electrostatics representations of apo-MlaC (PDB 6GKI) (25) revealing positively-charged patches (*blue surface*). Positively-charged residues (or groups of residues, *blue sticks*) are numbered from 0 to 7. (B) Representative immunoblots showing abolishment of disulfide crosslinks between MlaA and MlaC in Δ*mlaA* Δ*mlaC* cells expressing indicated surface charged-reversed mutants (numbered according to (A)) of cysteine-substituted MlaC-His and MlaA-His from pET22/42 and pCDF plasmids, respectively. (C) Representative immunoblots showing restoration of disulfide crosslinks between MlaA and

411 MlaC in Δ*mlaA* Δ*mlaC* cells expressing charge-reversed MlaC1-His and MlaA^{2DD2R}-His from pET22/42 and
412 pCDF plasmids, respectively. Samples were subjected to non-reducing (*top*) or reducing (*bottom*) SDS-PAGE
413 prior to immunoblotting. (D) Cartoon representations of Alphafold2-predicted MlaA (*teal*)-MlaC (*pink*) model,
414 revealing the proximity of residues D243/D244 on MlaA, and residues K84/R90 on MlaC illustrated in *blue*
415 and *red* sticks on MlaA and MlaC respectively (inset). Cutaway surface representation of this MlaA-MlaC
416 model is shown on the right, revealing the juxtaposition of the hydrophobic lipid-binding cavity of MlaC with
417 the hydrophilic channel of MlaA.
418

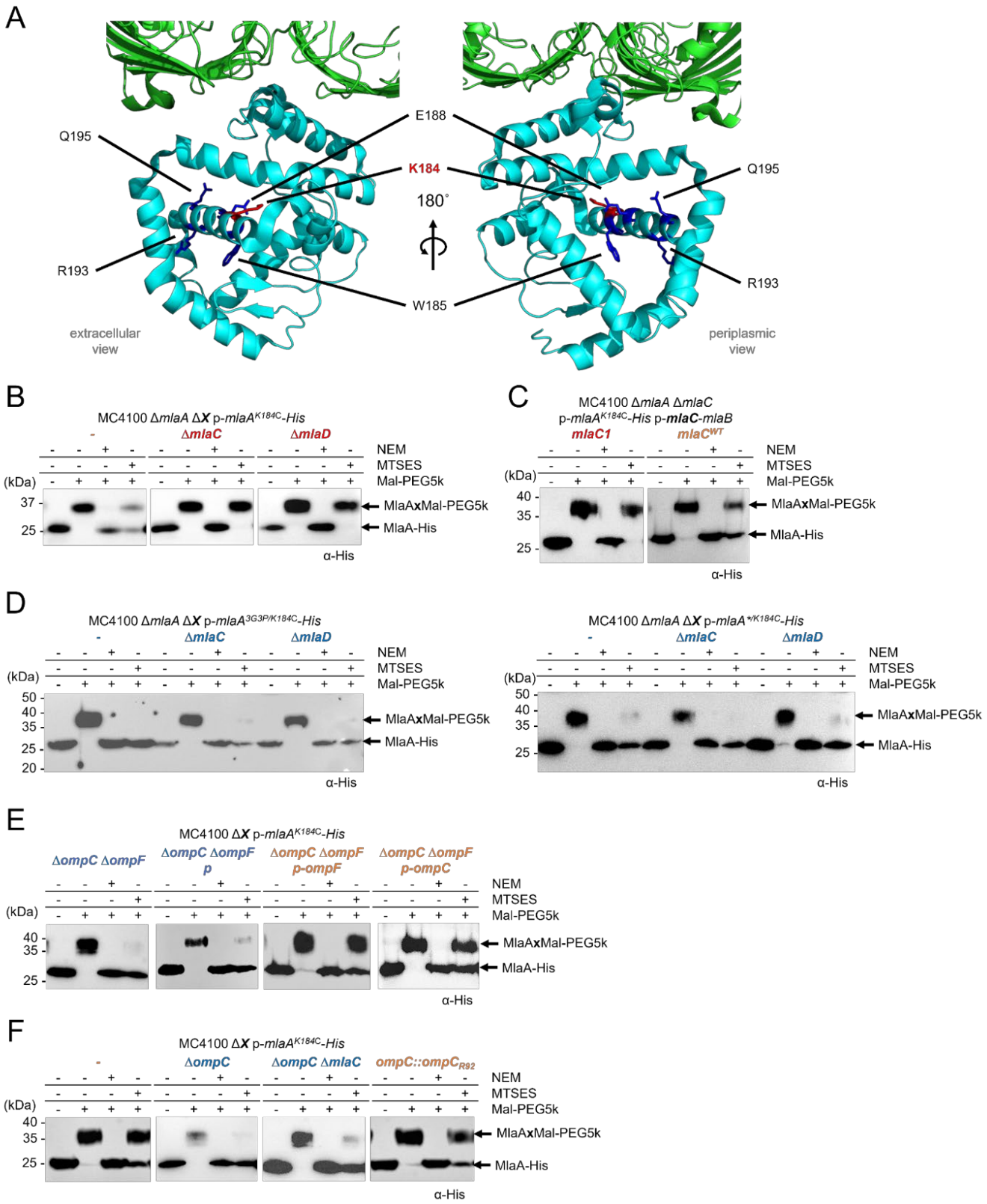

Figure 5. The MlaA hydrophilic channel exhibits solvent-accessibility changes due to interactions with MlaC and trimeric porins. Extracellular (*left*) and periplasmic (*right*) views of cartoon representations of the reported crystal structure of OmpK36 (*green*)-*Kp*MlaA (*cyan*) (PDB 5NUP) (32), showing channel residues substituted with cysteine (for SCAM) in *sticks*. (B, C) Representative immunoblots showing Mal-PEG5k alkylation of

424 MlaA^{K184C}-His cysteine variant expressed from the pCDF plasmid, either in (B) Δ*mlaA*, Δ*mlaA* Δ*mlaC*, and
425 Δ*mlaA* Δ*mlaD* backgrounds, or (C) Δ*mlaA* Δ*mlaC* background also producing wildtype or charge-reversed
426 K84D/R90D (MlaC1) MlaC variants from the pET23/43-*mlaCB* plasmid. (D) Representative immunoblots
427 showing Mal-PEG5k alkylation of MlaA^{K184C}-His variant also harboring non-functional 3G3P or gain-of-
428 function *mlaA** mutations expressed from pET23/42 plasmids in Δ*mlaA*, Δ*mlaA* Δ*mlaC*, and Δ*mlaA* Δ*mlaD*
429 background strains. (E, F) Representative immunoblots showing Mal-PEG5k alkylation of MlaA^{K184C}-His
430 cysteine variant expressed from the pCDF plasmid in various porin mutant backgrounds. In (E), OmpC or
431 OmpF were expressed from pDSW206 plasmids where indicated. In SCAM, cells were labelled with
432 membrane-permeable (NEM) or impermeable (MTSES) reagents, followed by alkylation with Mal-PEG5k,
433 which introduces a ~5-kDa mass shift to MlaA^{K184C}-His. The levels of solvent accessibility of K184C in MlaA
434 in the various strains, i.e. fully, partially, or not blocked by MTSES, are highlighted in *blue*, *orange*, or *red*,
435 respectively.
436

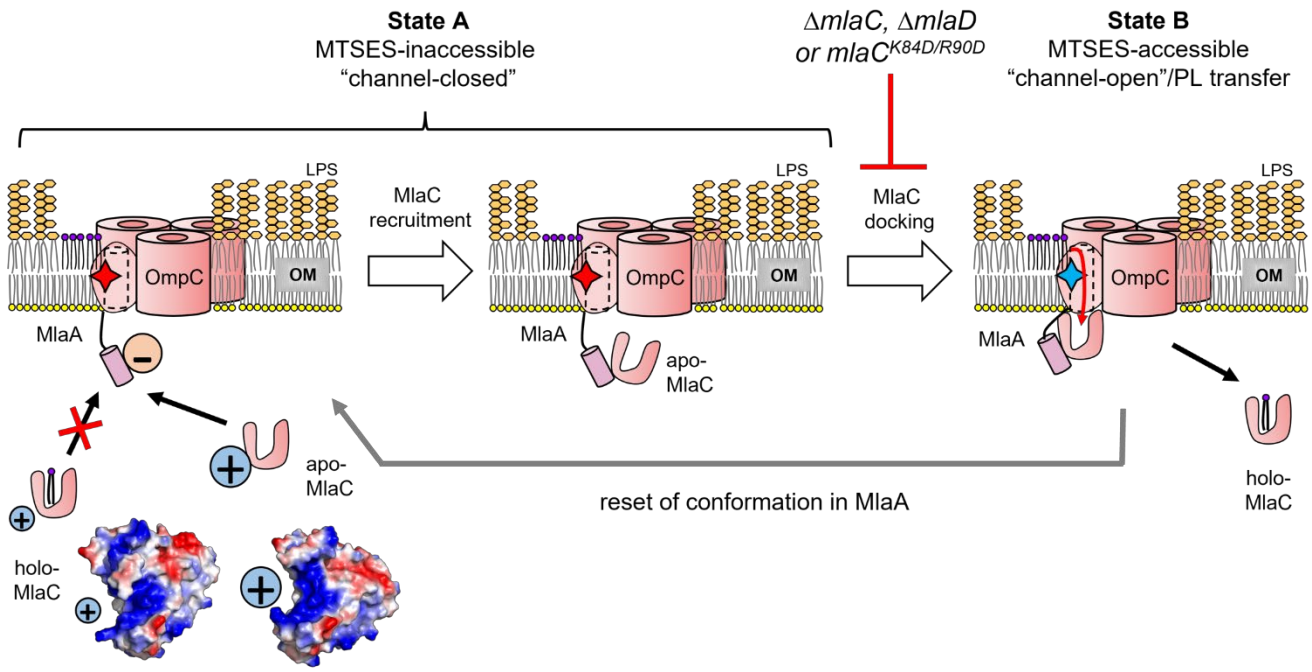

437

438 **Figure 6.** A proposed model for MlaC recruitment/binding and accompanying MlaA conformational changes
439 that facilitate retrograde PL transfer by the OmpC-MlaA-(MlaC) complex. At the OM, apo-MlaC is
440 preferentially recruited to MlaA via electrostatic interactions between MlaC surface charge patch and MlaA
441 C-terminal tail helix. Subsequent docking of MlaC to the base of the MlaA channel induces a conformational
442 change in MlaA, from an MTSES-inaccessible state (**State A**, "channel-closed", residue K184 represented by
443 *red star*) to an MTSES-accessible state (**State B**, "channel-open", residue K184 represented by *blue star*),
444 facilitating the transfer of PLs from the outer leaflet of the OM into the lipid binding cavity of MlaC. Holo-
445 MlaC then leaves the OmpC-MlaA complex to shuttle the PL ligand to the IM, thus resetting MlaA
446 conformation. Vacuum electrostatic surface representations of MlaC bound with lipids (PDB 5UWA) (23),
447 and in the unliganded form (PDB 6GKI) (25).

448